



**A HIGH-ENERGY MOLECULAR BEAM FACILITY
ADAPTED TO SATELLITE TEST AND DEVELOPMENT**

**W. B. Stephenson
ARO, Inc.**

**VON KÁRMÁN GAS DYNAMICS FACILITY
ARNOLD ENGINEERING DEVELOPMENT CENTER
AIR FORCE SYSTEMS COMMAND
ARNOLD AIR FORCE STATION, TENNESSEE 37389**

February 1974

Final Report for Period June 1, 1972 – July 31, 1973

Approved for public release, distribution unlimited.

Prepared for

**ARNOLD ENGINEERING DEVELOPMENT CENTER (XON)
ARNOLD AIR FORCE STATION, TENNESSEE 37389**

NOTICES

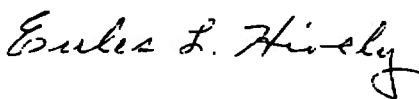
When U. S. Government drawings specifications, or other data are used for any purpose other than a definitely related Government procurement operation, the Government thereby incurs no responsibility nor any obligation whatsoever, and the fact that the Government may have formulated, furnished, or in any way supplied the said drawings, specifications, or other data, is not to be regarded by implication or otherwise, or in any manner licensing the holder or any other person or corporation, or conveying any rights or permission to manufacture, use, or sell any patented invention that may in any way be related thereto.

Qualified users may obtain copies of this report from the Defense Documentation Center.

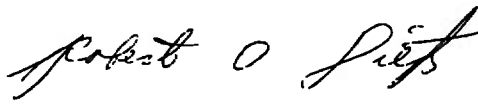
References to named commercial products in this report are not to be considered in any sense as an endorsement of the product by the United States Air Force or the Government.

APPROVAL STATEMENT

This technical report has been reviewed and is approved.



EULES L. HIVELY
Research and Development
Division
Directorate of Technology



ROBERT O. DIETZ
Director of Technology

SECURITY CLASSIFICATION OF THIS PAGE (When Data Entered)

DD FORM 1 JAN 73 1473 EDITION OF 1 NOV 65 IS OBSOLETE

UNCLASSIFIED

SECURITY CLASSIFICATION OF THIS PAGE (When Data Entered)

PREFACE

The research reported herein was conducted by the Arnold Engineering Development Center (AEDC) under sponsorship of the Air Force Cambridge Research Laboratories (AFCRL), Air Force Systems Command (AFSC) under Program Element 62101F. The results were obtained by ARO, Inc. (a subsidiary of Sverdrup & Parcel and Associates, Inc.), contract operator of AEDC, AFSC, Arnold Air Force Station, Tennessee. The work was done under Project No. VF230. The manuscript (ARO Control No. ARO-VKF-TR-73-136) was submitted for publication on October 1, 1973.

CONTENTS

	<u>Page</u>
1.0 INTRODUCTION	5
2.0 DESCRIPTION OF THE FACILITY	
2.1 Vacuum Chamber	6
2.2 Instrumentation	8
3.0 ADAPTATION OF THE FACILITY TO HYDROGEN BEAM OPERATION	
3.1 Hydrogen Pumping in the Test Section	10
3.2 Hydrogen Pumping in the Source Section	11
3.3 Beam Source and CO ₂ Distribution Cycling	13
4.0 BINARY BEAM CALIBRATION	
4.1 Beam Velocity	16
4.2 Species Flux	20
4.3 Beam Flux Variation in the Axial and Lateral Directions	29
5.0 CONCLUSIONS	30
REFERENCES	30

ILLUSTRATIONS

Figure

1. Satellite Incident Flux (Circular Orbit)	5
2. Molecular Beam Chamber	
a. Diagram of Chamber	7
b. Section through Source Section	7
3. Metastable Time-of-Flight Instrumentation	
a. Electron Gun	8
b. Time-of-Flight Schematic	9
4. Typical Metastable Time-of-Flight Records	
a. Argon - 2000°K, 611 torr, 53 μ sec/cm	9
b. (H ₂ + 1% Ar) - 285°K, 220 torr, 50 μ sec/cm.	9
c. (H ₂ + 1% Ar) - 2200°K, 590 torr, 20 μ sec/cm	9
d. H ₂ Beam - 2200°K, 785 torr, 20 μ sec/cm.	9
5. CO ₂ Frost Sorption of H ₂ in Beam-Test Section	11
6. CO ₂ Frost Sorption of H ₂ Jet-Source Section	12

<u>Figure</u>	<u>Page</u>
7. Source Section Pressure Rise During H ₂ Beam Flow	13
8. Cycling Gas Supply	14
9. Effect of Auxiliary Valve on Beam Pulse Shape—H ₂ + 1% Ar at 2000°K — 1cm/sec	
a. Beam Intensity - Auxiliary Valve Out, 300 torr Source Pressure	15
b. Auxiliary Valve Out, 1700 torr	15
c. Auxiliary Valve In, 1700 torr	15
10. Effect of Slip in Hydrogen-Xenon Beam	16
11. Heavy Species Limit Velocity and Energy in Seeded H ₂ Beams	18
12. Argon Velocity in H ₂ + 1% Ar Beams	19
13. Argon and Hydrogen Beam Intensities	22
14. Axial and Lateral Variations of Beam Intensity	23
15. Beam Intensities for H ₂ and (H ₂ + 1% Ar) Mixture	24
16. Binary (H ₂ + 1% Ar) Beam Component Flux	25
17. Metastable Argon in Beams	26
18. Room Temperature Beam Intensity - (H ₂ + 1% Ar) and H ₂ Beams	28
19. Argon Enrichment in H ₂ + 1% Ar Beam	29

APPENDIX

A. HYDROGEN SORPTION ON CO ₂ FROST	33
NOMENCLATURE	35

1.0 INTRODUCTION

The ability to perform development tests for satellite-carried instruments requires the generation of a higher velocity gas stream than what is possible by expansion into a vacuum from reservoir temperatures less than the melting point of any material. The velocity should lie in the range 7.3-7.8 km/sec so that particle energies will be from 4 to 20 eV for the common atmospheric species. Figure 1 shows the particle flux rate for a satellite as altitudes vary from 100 to 1000 km. The equivalent pressure indicates the background pressure in a test chamber at which the random strike rate is the same as the incident flux. This may set the upper limit in altitude for test simulation.

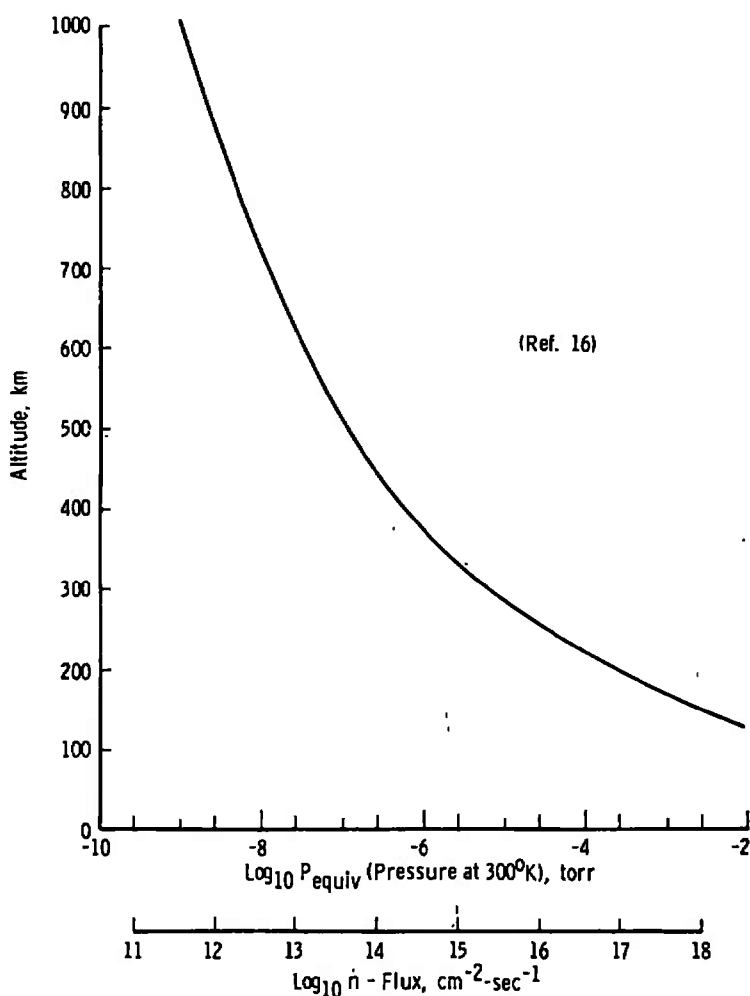


Figure 1. Satellite incident flux (circular orbit).

In addition to a realistic velocity (or energy) and flux rate, an adequate test facility will require a reasonably uniform stream about one centimeter in diameter with a flow duration of approximately one second.

It is feasible to produce a high-energy gas stream by seeding a hydrogen or helium molecular beam with a small fraction of a heavy species. Becker and Henkes (Ref. 1) and Abuaf (Refs. 2 and 3) have demonstrated that the theoretical velocity of the light species is attained by the heavier one.

Because of the stream size and flow duration requirements, the hydrogen pumping capacity must be two to three orders of magnitude greater than what is usual for the small laboratory beam system. Hydrogen pumping, therefore, was the major development effort.

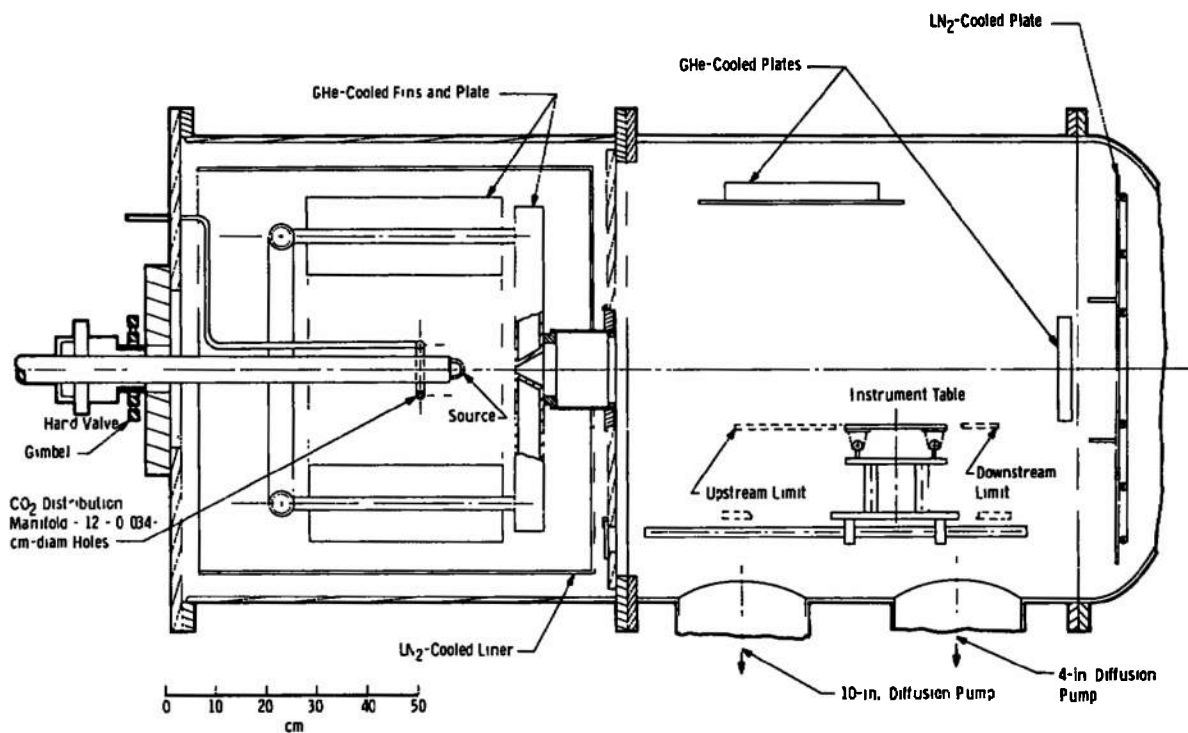
2.0 DESCRIPTION OF THE FACILITY

2.1 VACUUM CHAMBER

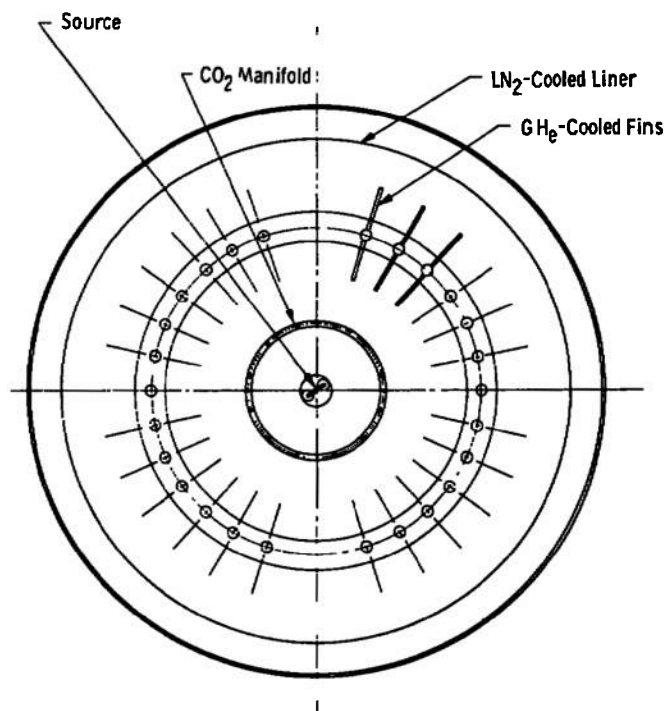
The test facility shown in section in Fig. 2 is a 1-m-diam, 2-m-long, stainless steel tank separated into two chambers by a bulkhead. Reference 4 gives a description of the molecular beam chamber in its original configuration. Several modifications have improved its general utility and have better adapted it to the present work:

1. The beam gas source is a U-shaped, resistance-heated, tantalum tube that can be inserted through a vacuum valve while the chamber is evacuated.
2. A finned cryogenic array in the source section provides the major fraction of the pumping.
3. A CO₂ addition system distributes the frost on cryogenic surfaces for hydrogen sorption.
4. An inbleed flow sequencing system supplies the beam gas alternately with CO₂ in order to maintain continuous hydrogen sorption pumping.

The collimator section of the conventional molecular beam configuration was eliminated to lengthen the usable test volume. For a cryogenically pumped chamber, the collimator section is not necessary.



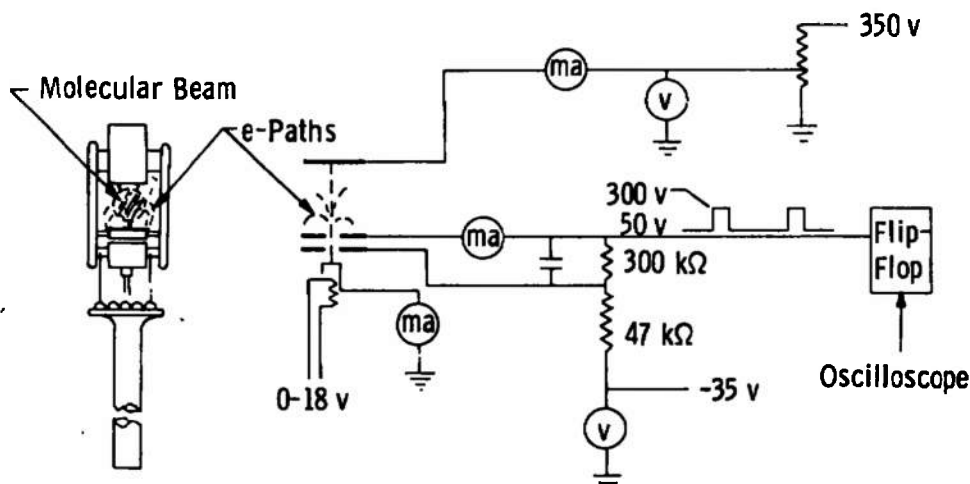
a. Diagram of chamber

b. Section through source section
Figure 2. Molecular beam chamber.

2.2 INSTRUMENTATION

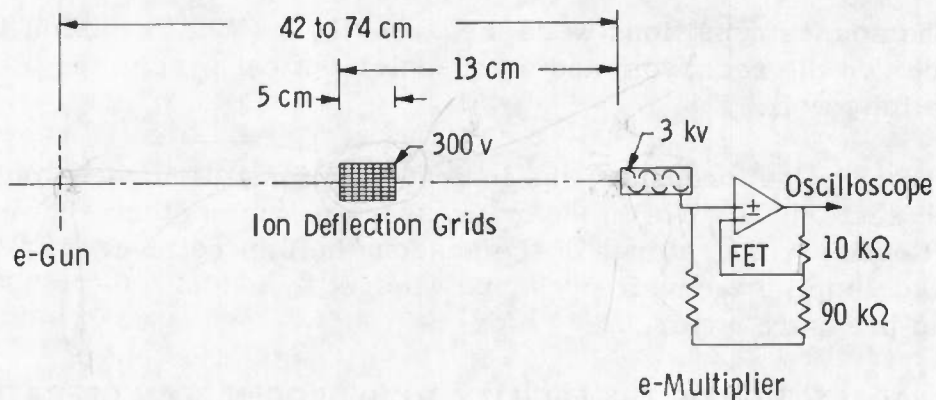
To calibrate the test stream, it is necessary to determine (1) beam intensity or total flux, (2) particle velocity, and (3) species concentration in the two-component beam. The instrumentation, which was mounted on a remotely movable table in the test section, consisted of a Bayard-Alpert-type ionization gage; a 13-stage, copper-beryllium electron multiplier; and a quadrupole mass spectrometer. The instrument table can be moved 32 cm axially and 11 cm transversely to bring the instruments into alignment with the beam.

The method of measuring beam particle velocity by detecting the metastably excited species, shown schematically in Fig. 3, was derived from Locke (Ref. 5). The large aperture (1.5 cm square) electron source was fabricated from a television picture tube gun by cutting off the last cylindrical element. Optimum metastable yields usually occur at relatively low electron energies (about 28 v for argon). A chopped metastable beam was generated by pulsing the electron accelerating voltage 1 to 20 μ sec at intervals comparable to the flight time. The time bases from a dual-beam oscilloscope formed the pulses, the duration of which were checked by a 10-MHz counter. A comparison of the times of flight for two distances showed that the electronics delays were negligible. Figure 4 shows some typical metastable time-of-flight records for various source conditions and gases. Argon has a strong signal in the binary beam, whereas hydrogen alone gives a very small signal (Fig. 4d).

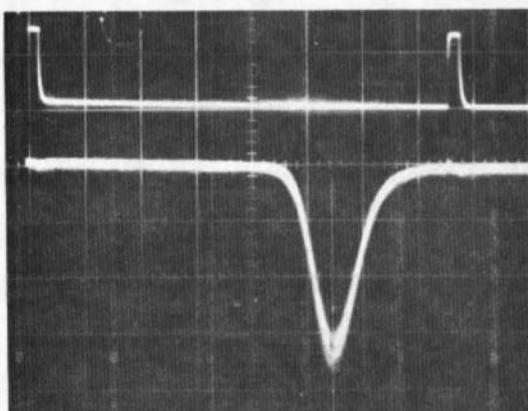


a. Electron gun

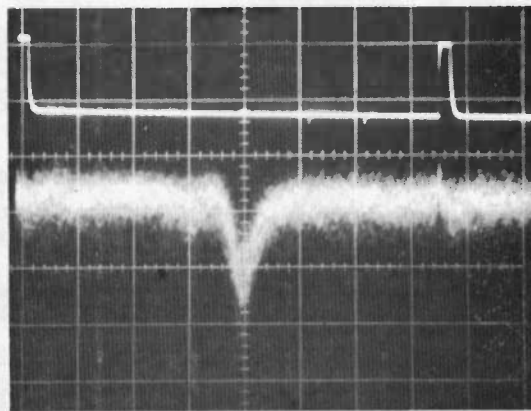
Figure 3. Metastable time-of-flight instrumentation.



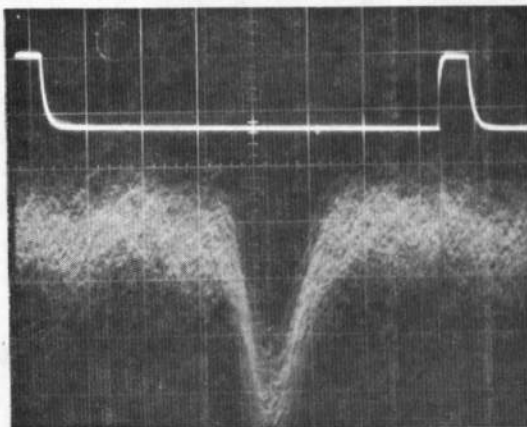
b. Time-of-flight schematic
Figure 3. Concluded.



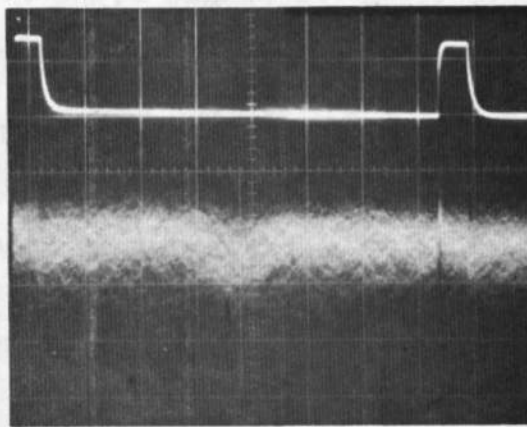
a. Argon—2000° K, 611 torr, 53 μ sec/cm



b. ($H_2 + 1\% \text{ Ar}$) - 285° K, 220 torr, 50 μ sec/cm



c. ($H_2 + 1\% \text{ Ar}$) - 2200° K, 590 torr, 20 μ sec/cm



d. H_2 beam - 2200° K, 785 torr, 20 μ sec/cm

Figure 4. Typical metastable time-of-flight records.

The source conditions were measured by a CEC Precision Pressure Balance® on the reservoir and a two-color optical pyrometer viewing the source tube wall.

The chamber pressure was indicated by ionization gages on the walls of each section. Hydrogen vapor pressure thermometers showed the inlet and outlet temperatures of the gaseous helium refrigerant. CO₂ manifold supply reservoir pressure was set by use of a 0- to 800-torr aneroid pressure gage.

3.0 ADAPTATION OF THE FACILITY TO HYDROGEN BEAM OPERATION

3.1 HYDROGEN PUMPING IN THE TEST SECTION

Although the test section has 4- and 10-in. diffusion pumps, its primary pumping comes from the two cryogenic surfaces cooled by a 4-kw gaseous helium refrigerator. For a hydrogen beam flux of 10^{17} molecules/sec (2.8×10^{-3} torr-ℓ/sec), the 10-in. diffusion pump would give a minimum pressure of 1.5×10^{-6} torr. For the present application, this is two orders of magnitude higher than desirable.

Appendix A shows that an equilibrium pressure of 10^{-8} torr hydrogen can be maintained if 20 to 50 moles of CO₂ per mole of H₂ are deposited on a cryosurface at 15 to 20°K. The actual transient pressure during beam flow appears to be determined by the strike rate on the frost surface. For instance, if one assumes the above 2.8×10^{-3} torr-ℓ/sec inflow rate to 1000 cm² cryosurface, the minimum chamber pressure corresponding to the strike rate ($3.64 \times 10^3 \sqrt{T/M}$ ℓ/sec/cm²) will be 4×10^{-8} torr.

Figure 5 is an operating chart to determine the flow time for CO₂ inbled to the test section at 5×10^{-5} torr which provides 40 molecules CO₂ for each H₂. Figure A-2 indicates that one can expect an equilibrium pressure of 10^{-8} torr for a frost temperature of 17°K and 10^{-6} torr at 19°K. The usual operating procedure was to close the diffusion pumps and bleed in CO₂ for 10 to 15 minutes at 5 to 6×10^{-5} torr. With a beam flow time of 1 sec, several hundred beam pulses could be absorbed before the frost required renewal. This could be done by depositing a new frost layer or by warming the frost to 20 to 22°K (Refs. 6 and 7).

In practice, the test section remained below a pressure of 5×10^{-7} torr during all beam flows. The lowest base pressure without flow was

2×10^{-8} torr. Normally, it was unnecessary to renew the frost during the running time of a day unless beam gases other than hydrogen covered the CO_2 frost and reduced its sorption ability. Reference 7 notes this effect on frost sorption for hydrogen pumping.

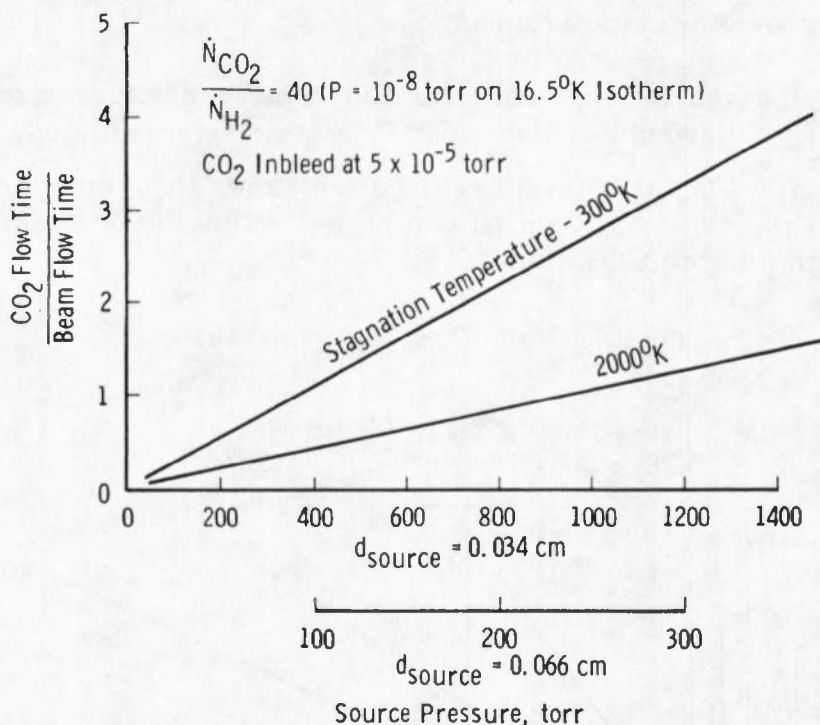


Figure 5. CO_2 frost sorption of H_2 in beam-test section.

3.2 HYDROGEN PUMPING IN THE SOURCE SECTION

The hydrogen pumping required in the source section is 99.8 percent of the total source flow and is therefore the most difficult. A source section pressure as high as 10^{-4} torr can be tolerated since a source stagnation pressure of 1000 torr results in a ratio of 10^7 , enough to provide a large isentropic core in the free-jet expansion.

The cryosurface geometry shown in Figs. 2a and b is particularly adapted to the cryopumping of a free-jet flow field. The end wall is coldest at the center where the refrigerant inlet is located. The beam is formed at this point by the orifice, which acts as the skimmer in a conventional molecular beam system. The finned array maintains a low background by providing a large surface area and allowing the incident gas to pass through it and be cooled by the liquid-nitrogen-filled shroud behind it before striking the fins.

To use this array for CO₂ frost sorption pumping of hydrogen, it was necessary to locate the injection orifices off the axis so that the fins would be coated without covering the LN₂-cooled liner. A toroidal manifold with 12 holes was mounted concentric with the axis of the chamber. The source could be moved through it for alignment or varying the source-skimmer distance.

Figure 6 gives the flow time for CO₂ when a conservative ratio ($\dot{N}_{\text{CO}_2}/\dot{N}_{\text{H}_2} = 20$, where \dot{N} = number flux (sec⁻¹) is selected. Typically, a flow time for CO₂ at 200 torr will be ten times that for hydrogen. An electronic timer was built which controlled solenoid valves alternately for the beam and the CO₂ supplies.

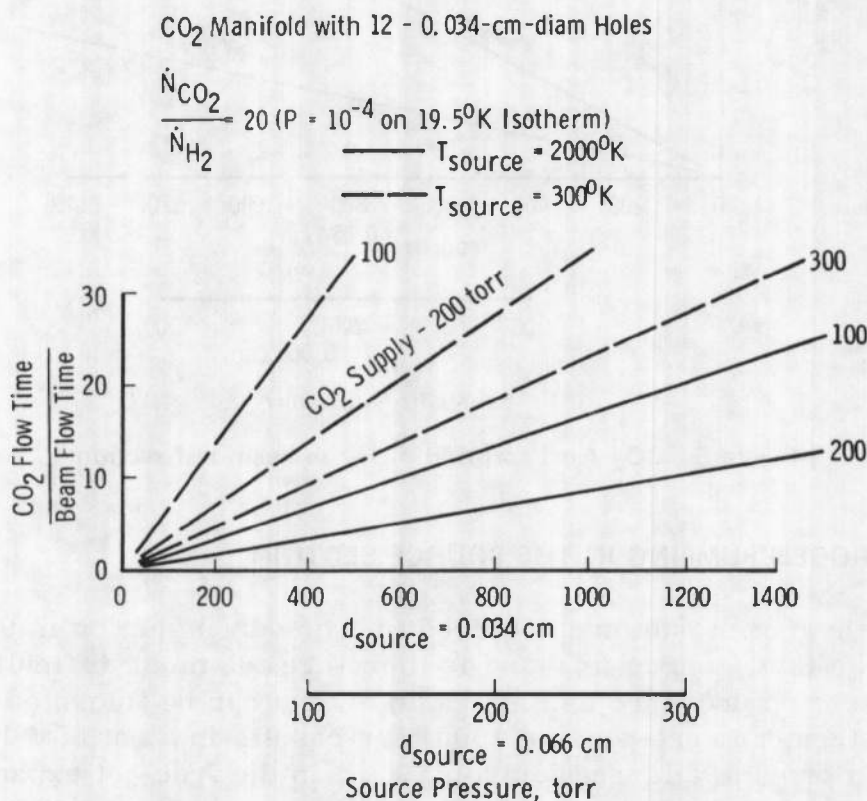


Figure 6. CO₂ frost sorption of H₂ jet-source section.

During several of the development tests, some peak source section pressures were observed, as shown in Fig. 7. These are reasonably consistent with the equilibrium pressures for various CO₂/H₂ concentrations. The actual frost temperature was unknown but fell within the range from 16 to 20°K. It is evident that the 20:1 ratio of CO₂ to H₂ will usually result in pressures less than 10⁻⁴ torr.

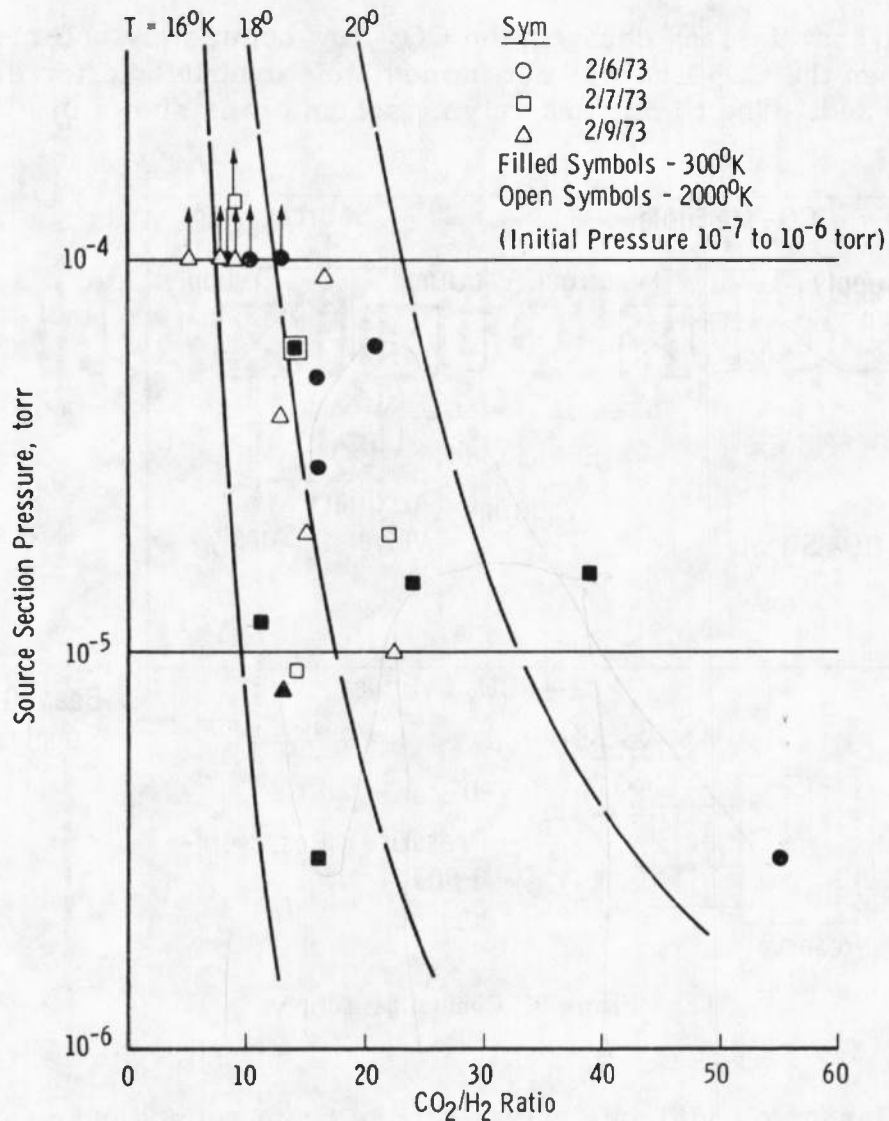


Figure 7. Source section pressure rise during H_2 beam flow.

3.3 BEAM SOURCE AND CO_2 DISTRIBUTION CYCLING

Hagena (Ref. 8) demonstrated the feasibility of pulsing a molecular beam source flow in order to obtain high fluxes with modest vacuum pumping capacity. His valving provided millisecond-duration beams and was not directly applicable to a high-temperature source. In order to produce a reasonably rectangular beam pulse when the valve is located remote from the orifice, it is necessary to operate alternately two valves—one to the supply reservoir and the other to vacuum. It was

observed that the long decay in the CO₂ flow completely obliterated the beam when the CO₂ line was not immediately evacuated after the supply valve closed. The timing and valving schematic is shown in Fig. 8.

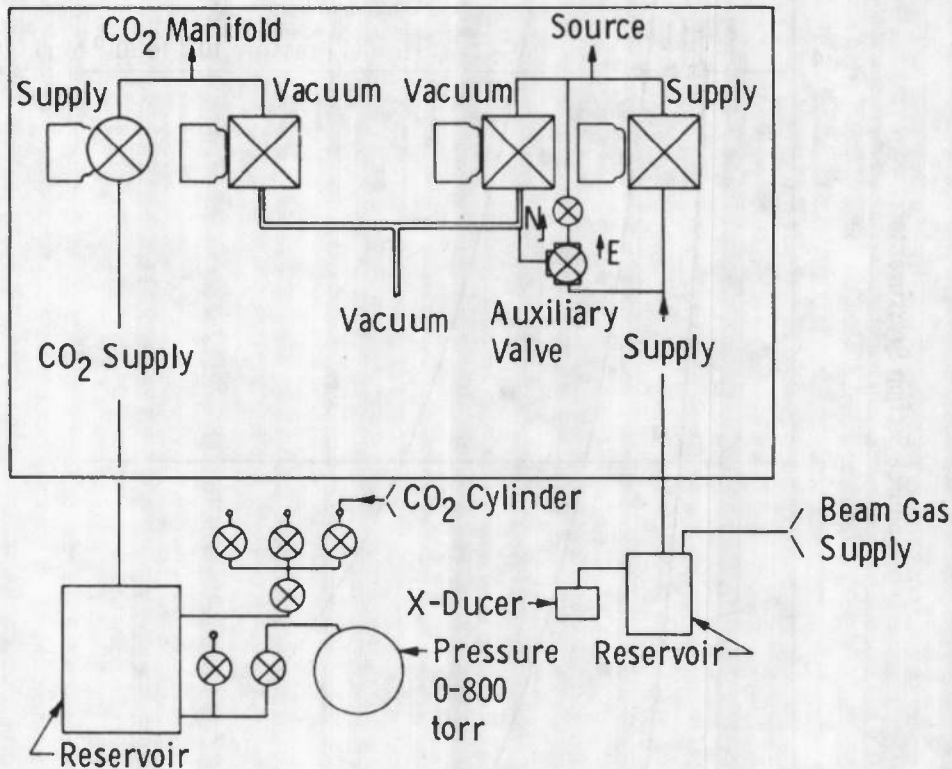
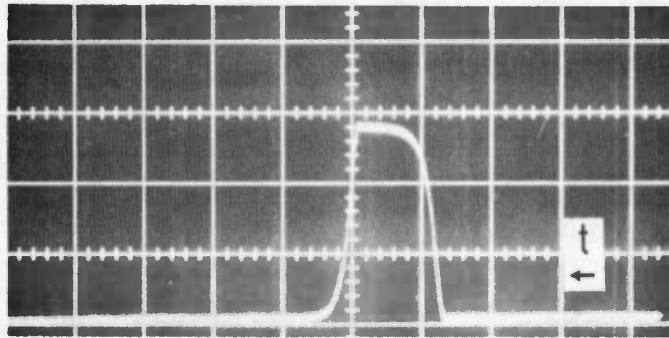
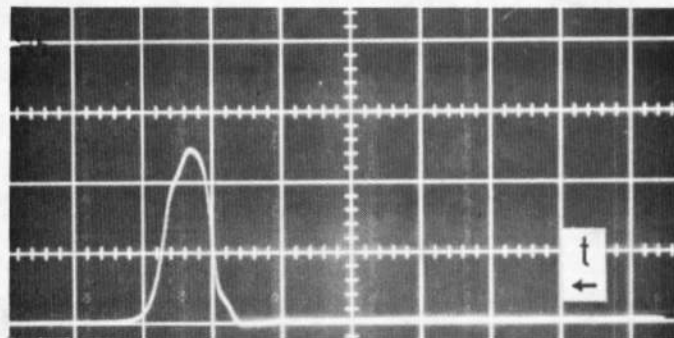


Figure 8. Cycling gas supply.

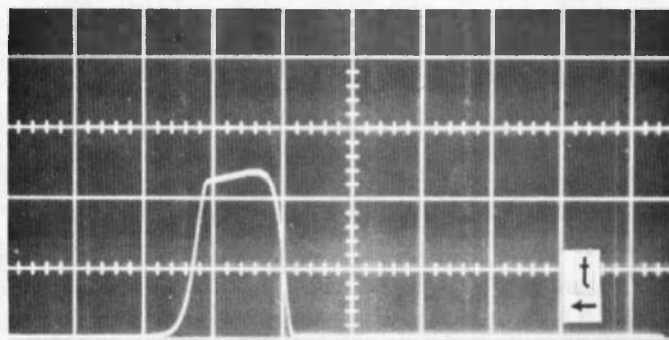
The large solenoid gate valves for the beam supply and evacuation operated sluggishly when the pressure exceeded an atmosphere. A small orifice two-way solenoid auxiliary valve, installed in parallel with the large gate valves, eliminated this difficulty. Figure 9 shows the effect of energizing this valve simultaneously with the supply gate valve. A beam ($H_2 + 1\% Ar$) from a 2000°K source produced an ionization gage signal that was displayed on the oscilloscope at 1 cm/sec. Figure 9a shows a full second pulse with a 300-torr source pressure. When the pressure is 1700 torr (Fig. 9b), the beam is delayed by slow opening of the valve. Figure 9c shows that the auxiliary valve operates quickly by dropping the pressure across the gate valve and allowing it to open.



a. Beam intensity—auxiliary valve out,
300 torr source pressure



b. Auxiliary valve out, 1700 torr



c. Auxiliary valve in, 1700 torr

Figure 9. Effect of auxiliary valve on beam pulse
shape— $H_2 + 1\% Ar$ at $2000^\circ K$ — 1 cm/sec .

4.0 BINARY BEAM CALIBRATION

4.1 BEAM VELOCITY

As the findings in Ref. 2 demonstrate, the velocity of the heavier species of a seeded beam approaches the limiting thermal velocity as the Knudsen number (defined as source diameter divided by mean free path of the hydrogen at stagnation conditions) becomes small. Figure 10 shows this deviation from the thermal limit as a function of inverse Knudsen number.

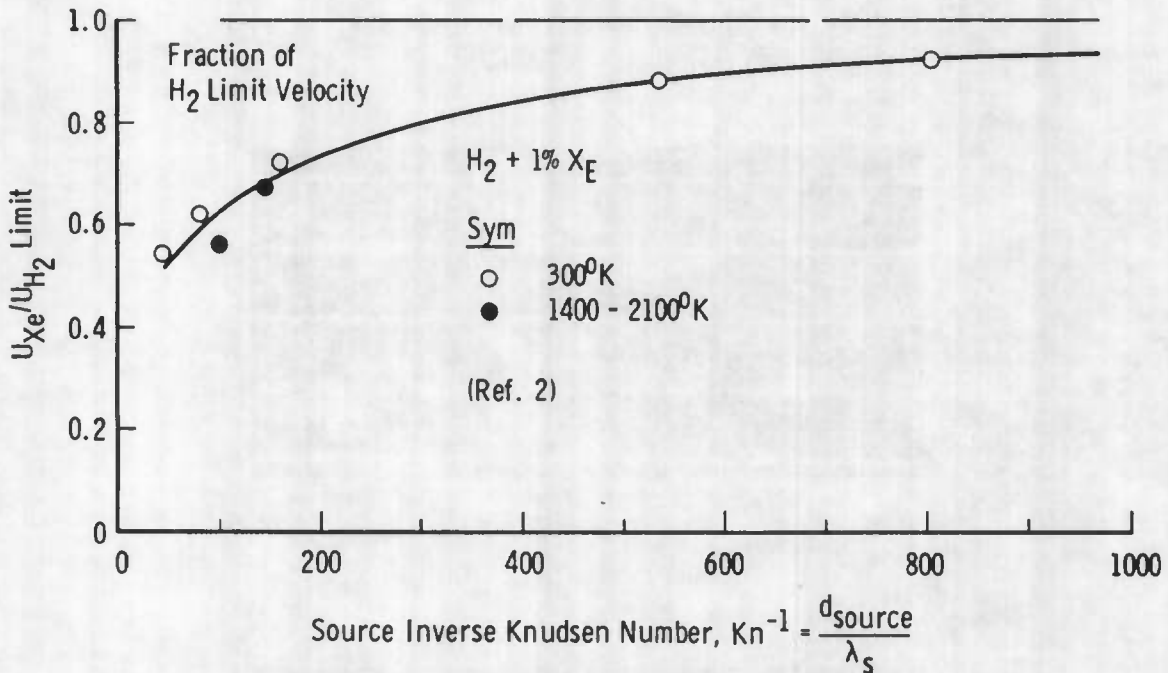


Figure 10. Effect of slip in hydrogen-xenon beam.

Reference 2 showed that beam mixtures of helium with small amounts of a heavy species approached the theoretical limit speed $[U_{lim} = (\sqrt{2\bar{\gamma}/\bar{\gamma} - 1})(kT_T/\bar{m})]$ for a mean molecular mass, \bar{m} , and weighted specific heat ratio, $\bar{\gamma}$, where k is the Boltzmann constant and T_T is the stagnation temperature. However, hydrogen, pure or with a seed species, had slightly lower velocities than what would be calculated for a diatomic ($\gamma = 1.4$) gas expansion. This is attributed to rotational nonequilibrium, and velocities calculated by assuming rotational freezing at sonic conditions are in close agreement with measurements. To calculate the thermal limit speed for hydrogen, one assumes that a

diatomic ($\gamma = 7/5$) expansion starts from T_T . When the temperature and velocity correspond to sonic conditions for a monatomic expansion ($\gamma = 5/3$), the subsequent acceleration approaches a limit as if the stagnation temperature were T_T' . The energy equation is written

$$\frac{u^2}{2} + \frac{\gamma}{\gamma-1} \frac{kT}{m} = \frac{\gamma}{\gamma-1} \frac{kT_T}{m}$$

and the isentropic sonic speed and temperature are

$$u^* = \sqrt{\frac{2\gamma}{\gamma-1} \frac{kT_T}{m}} \quad \text{and} \quad T^* = \frac{2}{\gamma+1} T_T$$

If the sonic conditions above are written for $\gamma = 5/3$ and $T_T = T_T'$, they can be substituted in the energy equation for $\gamma = 7/5$. The effective stagnation temperature will be $T_T' = (14/13)T_T$. When this is substituted into the limit thermal velocity formula for $\gamma = 5/3$, the ultimate speed for hydrogen or binary beams with small amounts of a heavy species is given by

$$U_{lim} = \sqrt{(70/13) kT_T/m}$$

or

$$U_{lim} = 2.115 \times 10^4 \sqrt{T_T/\bar{M}}$$

which can be compared with $U_{lim} = 2.41 \times 10^4 \sqrt{T_T/\bar{M}}$ for an ideal diatomic expansion ($\gamma = 7/5$). Figure 11 shows beam velocity for various binary mixtures.

100% H_2	$U_{lim} = 1.51 \times 10^4 \sqrt{T_T/\bar{M}} \quad \bar{M} = 2$
99% H_2 + 1% Ar	$U_{lim} = 1.37 \times 10^4 \sqrt{T_T/\bar{M}} \quad \bar{M} = 2.38$
95% H_2 + 5% Ar	$U_{lim} = 1.07 \times 10^4 \sqrt{T_T/\bar{M}} \quad \bar{M} = 3.90$
99% H_2 + 1% Xe	$U_{lim} = 1.165 \times 10^4 \sqrt{T_T/\bar{M}} \quad \bar{M} = 3.29$

where \bar{M} is the mean molecular weight. The heavy particle kinetic energy in electron-volts is given by

$$E = 5.19 \times 10^{-13} \bar{M} U_{lim}^2$$

which is also shown in Fig. 11. At 2000°K the 1-percent argon mixture has a maximum energy of about 8 ev and the xenon has nearly 20 ev.

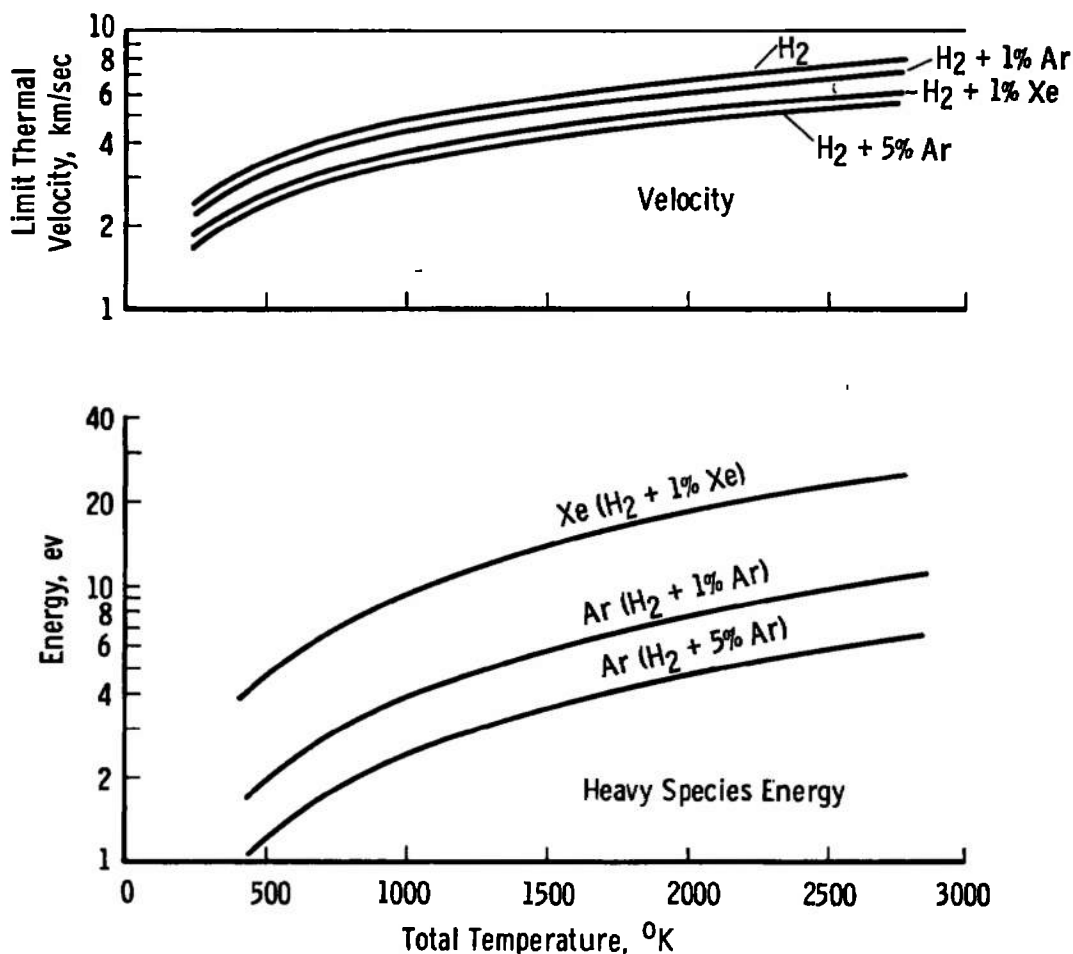


Figure 11. Heavy species limit velocity and energy in seeded H_2 beams.

The experimental velocities can be compared to velocities calculated from the limit speed corrected by the slip factor (Fig. 10). Figure 12 shows this for different source diameters and stagnation conditions. The experimental velocities of the argon species were determined by the time of flight of metastable atoms over a 42-cm distance. Figure 4 shows several typical oscilloscope traces that provided times of flight.

The choice of an orifice size is a compromise among pumping capacity in the source section, slip of the heavy species at large Knudsen number, and pressure limits of the source system. Since the source flow is proportional to the square of the orifice diameter and the Knudsen number is inversely proportional, it is desirable to use a small orifice at high pressure.

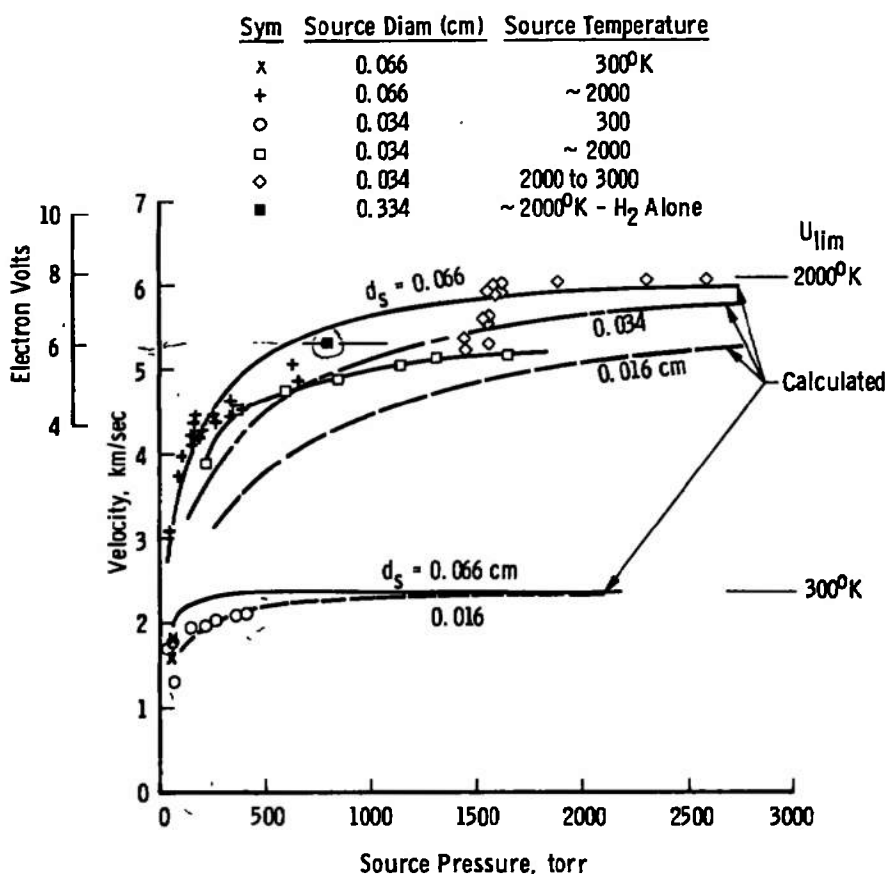


Figure 12. Argon velocity in H₂ + 1% Ar beams.

The flight speeds at an indicated source temperature of 2200°K (by optical pyrometer) suggest that the actual stagnation temperature is close to 1500°K. As the temperature is raised toward 3000°K, the velocity approaches 6.1 km/sec, which corresponds to a 2000°K stagnation temperature. Part of this deviation is the result of cooling of the tube wall during gas flow; the recorded temperature is for no flow, and a 50 to 60°C drop was observed during flow. When argon is flowed at the same pressure, there is no perceptible drop in temperature. Since the molar flow is $\sqrt{20}$ times greater for hydrogen and the molar specific heat is 7/5 greater, over 6 times as much heat is required to raise the temperature of hydrogen compared with argon.

The tendency for the argon velocity to be higher than calculated at low source pressure is probably because the slip correction (Fig. 10) was derived for xenon and may be excessive. As temperature and pressure are raised, the velocity approaches the calculated limit of 6.1 km/sec corresponding to 2000°K stagnation temperature.

4.2 SPECIES FLUX

The individual species fluxes in the hydrogen-argon beam were estimated by two measurements: (1) the ion current in an ionization gage and (2) the signal from an electron multiplier calibrated for metastable argon. In the first method, the ion current is compared for the binary beam and the pure hydrogen beam. The second method required the pure argon beam to calibrate the detector, which is practically sensitive only to argon metastables, and to use this calibration to determine the argon concentration in the seeded beam.

4.2.1 Ion Gage Determination

The glass-envelope miniature ionization gage had its entrance closed by a plate with a 0.64-cm-diam thin-edge orifice through which the center of the beam entered. From the conservation of mass flux (Ref. 9), the pressure in the gage is related to the influx by

$$\dot{n} = 3.51 \times 10^{22} \frac{P}{\sqrt{M T_g}}$$

where

$$\begin{aligned}\dot{n} &= \text{number flux (cm}^{-2}\text{sec}^{-1}\text{)}, \\ P &= \text{pressure, and} \\ T_g &= \text{ion gage temperature}\end{aligned}$$

or if T_g is taken as 300°K,

$$\dot{n} = 2.025 \times 10^{21} P / \sqrt{M}$$

When a gage is calibrated to read a pressure, P_g , proportional to the ion current for nitrogen, the flux is given in terms of a sensitivity factor S_B :

$$\dot{n} = 2.02 \times 10^{21} (S_{N_2}/S_B) P_g / \sqrt{M_B}$$

Then for hydrogen, $S_{N_2}/S_{H_2} = 2.14$

$$\dot{n} = 3.06 \times 10^{21} P_g$$

and for argon, $S_{N_2}/S_{Ar} = 0.84$

$$\dot{n} = 2.69 \times 10^{20} P_g$$

The hydrogen sensitivity factor has been checked experimentally with nitrogen and hydrogen beams and that for argon is from Ref. 9.

The flux from a free jet exhausting into a vacuum on the axis (see Ref. 10 or 11) can be expressed per unit solid angle as

$$\dot{N}/\omega = \dot{N}^* f(\gamma)$$

where ω is the solid angle (steradian) and N^* is the total flow from the source:

$$\dot{N}^* = n^* u^* A^* = (2/\gamma + 1)^{\frac{\gamma+1}{2(\gamma-1)}} \rho_1 a_1 (N_A/\lambda) A^*$$

where A^* is the area of sonic orifice, ρ is mass density, and a is acoustic speed.

The factor $\rho_T a_T$ is the density and acoustic speed at the source stagnation conditions. By introducing the Avogadro number (N_A), standard pressure, and temperature, one can write

$$\dot{N}/\omega = 2.62 \times 10^{22} \frac{P_T A^*}{\sqrt{M T_T}} \text{ per steradian for } \gamma = 1.40$$

and

$$\dot{N}/\omega = 4.03 \times 10^{22} \frac{P_T A^*}{\sqrt{M T_T}} \text{ for } \gamma = 5/3$$

$$(P_T \text{ in torr and } T_T \text{ in } ^\circ\text{K})$$

Since \dot{n} , the flux per unit area, is equal to $(\dot{N}/\omega)/\ell^2$, the above expressions times ℓ^{-2} can be equated to the number flux in terms of ion gage reading to give for argon and hydrogen:

$$\text{Argon: } P_g = 23.6 \frac{P_T A^*}{\ell^2 \sqrt{T_T}}$$

and

$$\text{Hydrogen: } P_g = 6.05 \frac{P_T A^*}{\ell^2 \sqrt{T_T}}$$

These are shown in Fig. 13 with experimental data for typical single-species beams. The argon signal is lower than the calculated intensity by a factor of about 3 and hydrogen by about 2. Part of this attenuation is obviously the migration of beam particles away from the axis after skimming has formed the beam. For example, the radial distribution of intensity at 77 cm, shown in Fig. 14, may be integrated with radius to yield a total proportional to the beam particle flux. If this is divided by the geometrical area of the beam defined by the collimating orifices, the intensity which results is 1.9 times the measured beam intensity on the centerline. The pulsed operation mode for argon (1 sec flow and 15 sec off) is the same as for the hydrogen binary beam. It appears that the pulsed mode gives a higher intensity beam because of skimmer interaction. Transient effects in cryogenic pumping are discussed in Ref. 12, and hence a decrease in pumping at the skimmer orifice under steady conditions might be anticipated.

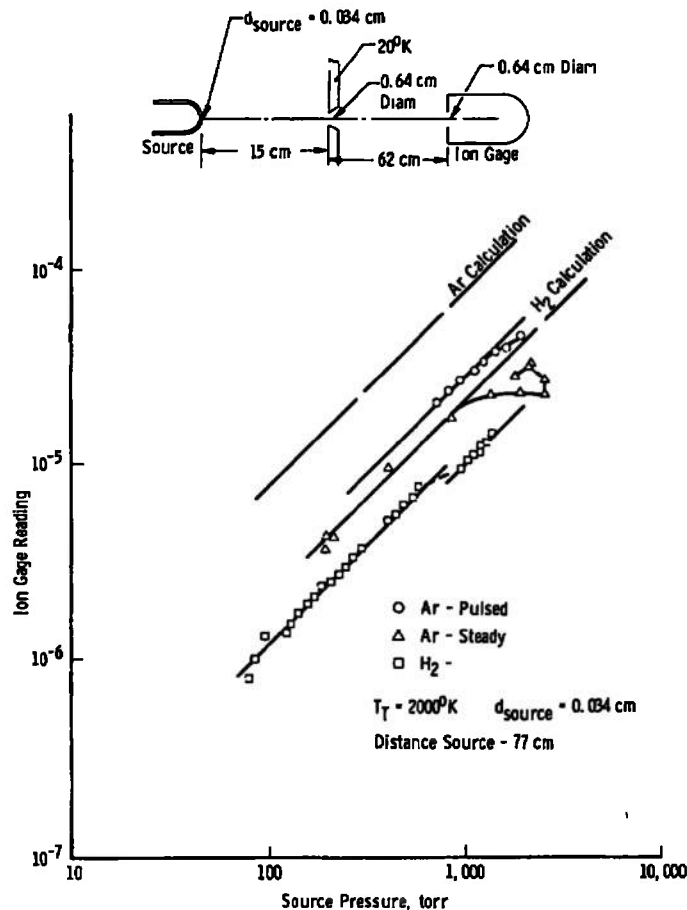


Figure 13. Argon and hydrogen beam intensities.

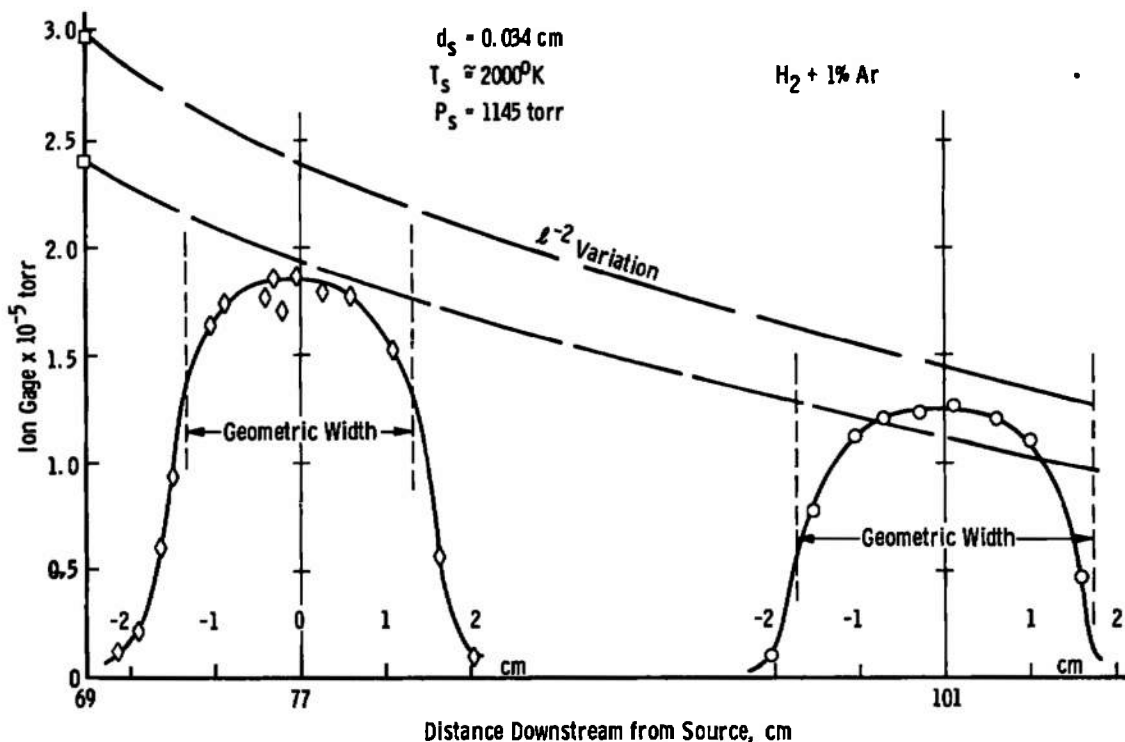


Figure 14. Axial and lateral variations of beam intensity.

There is a distinct break in the hydrogen and hydrogen-argon beam intensities at about 1000 torr that is closely related to skimmer effects. For the 0.66-mm source diameter, it occurs at about 250 torr, which shows that there is a loss of cryosorption pumping at strike rates greater than about 10^{18} molecules of hydrogen per second per square centimeter (an ion gage at the skimmer location would read 2.5×10^{-4} torr). The observed pressure varies somewhat with cryosurface temperature, which was between 14 and 19°K.

Figure 15 is a comparison of the beam intensity observed for hydrogen and for 1-percent argon in hydrogen at two distances from the source. The deviation noted above occurs at 800- to 1000-torr source pressure for all four runs.

The induction of species fluxes from the ion gage readings proceeds as follows. The ion gage output is directly proportional to the source pressure and an empirical formula can be written to fit the data,

$$P_g = \text{const} \times P_{\text{source}}$$

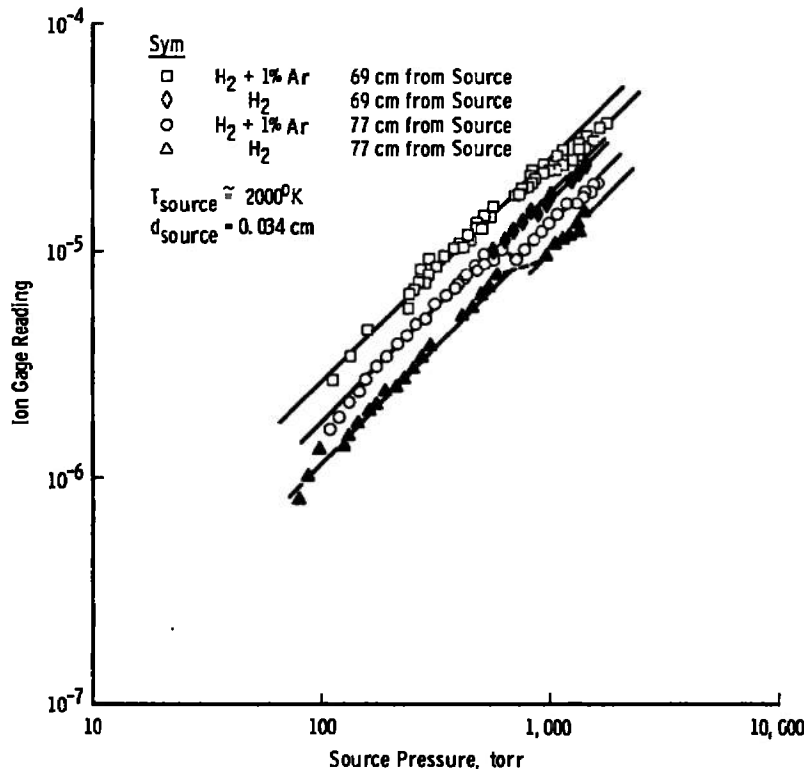


Figure 15. Beam intensities for H₂ and (H₂ + 1% Ar) mixture.

It is assumed that the total ion current is the sum of the individual component species in the gage, $P_{g\text{H}_2 + \text{Ar}} = \Delta P_{g\text{H}_2} + \Delta P_{g\text{Ar}}$. The hydrogen partial current, $\Delta P_{g\text{H}_2}$, can be derived from the pure hydrogen beam by assuming that it is modified only by the decreased source flux, \dot{N}^*

$$\dot{N}^* = n_T A_T f(\gamma) \sim \left(\frac{n_{\text{H}_2}}{n_{\text{H}_2} + n_{\text{Ar}}} \right)_{\text{source}} \sqrt{2/M}$$

where the first term is the fraction of hydrogen in the source mixture and the acoustic speed is a function of \bar{M} , the mean molecular weight of the source mixture. The fraction of hydrogen in the argon-hydrogen beam mixture is therefore

$$\frac{(n_{\text{H}_2})_{\text{H}_2 + \text{Ar}}}{(n_{\text{H}_2})_{100\% \text{ H}_2}} = 0.99 \sqrt{2/2.38} = 0.906$$

and

$$\Delta P_{H_2} = 0.906 P_{H_2}$$

Then the argon fraction is

$$\Delta P_{Ar} = P_g - \Delta P_{H_2}$$

and the individual fluxes are

$$\dot{n}_{H_2} = 3.06 \times 10^{21} \Delta P_{H_2}$$

$$\dot{n}_{Ar} = 2.69 \times 10^{20} \Delta P_{Ar}$$

Figure 16 shows the results of the data analysis for 1-percent hydrogen beams measured at two positions in the test region. It appears that the attenuation is greater for argon than for hydrogen when skimmer interaction occurs at the high pressures.

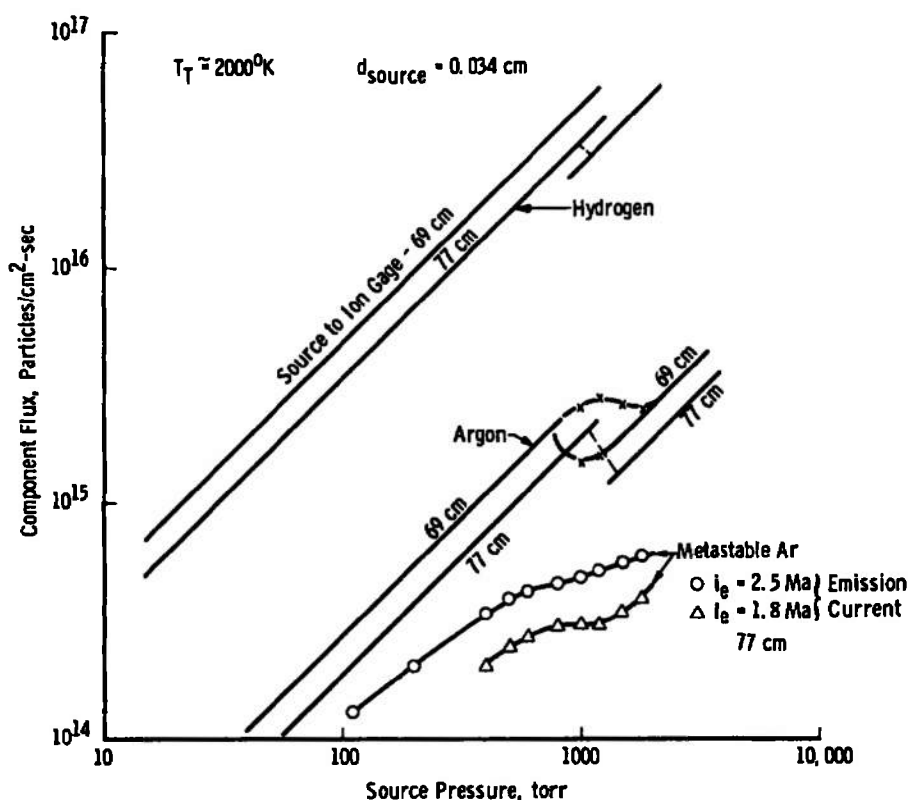


Figure 16. Binary (H₂ + 1% Ar) beam component flux.

4.2.2 Argon Flux from Metastable Signal

Figure 17 shows the electron multiplier signals on an arbitrary scale for metastable argon. As Fig. 4 shows, the metastable hydrogen signal is very small compared to that for argon. The binary beam signals show a deviation that may be the result of electron depletion by the hydrogen molecules rather than a decrease in argon flux.

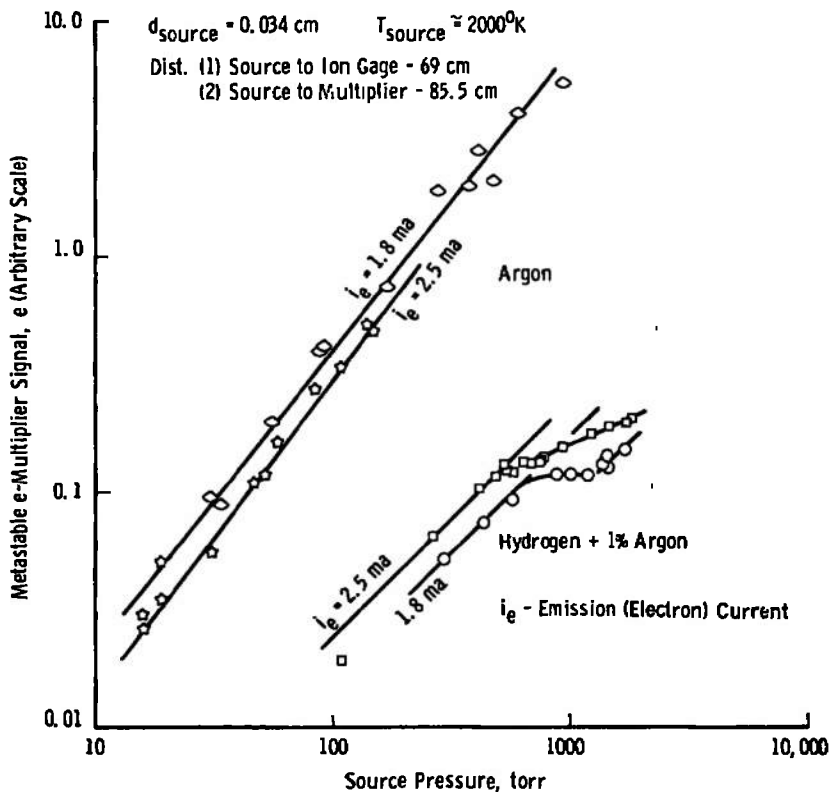


Figure 17. Metastable argon in beams.

The signal for the pure argon beam can be fitted by curves of the form,

$$\begin{array}{lll} e = 1.075 P^{1.285} & i_e = 1.8 \text{ ma} & \text{emission current} \\ e = 0.591 P^{1.353} & i_e = 2.5 \text{ ma} & \text{emission current} \end{array}$$

The relation between argon number flux and source pressure was given before as

$$\dot{n}_{Ar} = 2.69 \times 10^{20} P_{g_{Ar}}$$

The ionization gage signal from Fig. 13 can be fitted by

$$P_g = 2.85 \times 10^{-8} P_{\text{source}}$$

for a 77-cm distance from the source. The combination of the above equations provides the calibration formulas:

$$\begin{aligned} \dot{n}_{\text{Ar}} &= 2.38 \times 10^{15} e^{0.778} & i_e &= 1.8 \text{ ma} \\ \dot{n}_{\text{Ar}} &= 2.85 \times 10^{15} e^{0.74} & i_e &= 2.5 \text{ ma} \end{aligned}$$

When these factors are applied to the metastable signal of the binary ($\text{H}_2 + 1\% \text{ Ar}$) beam, the argon flux is as shown in Fig. 16.

The argon in the binary beam, as determined from the metastable signal, is about half of that derived from the ionization gage at low pressures and drops to a quarter at 1000 torr (Fig. 16). In addition, a decrease in electron current from 2.5 to 1.8 ma reduces the metastable argon signal 40 percent. The preceding considerations lead to the conclusion that the metastable signal method of deriving the heavy species flux in a binary beam is not practicable. Apparently, the hydrogen in the beam scatters or absorbs some of the exciting electrons and reduces the metastable yield. Note (Fig. 17) that an increase in electron emission current results in more metastables in the binary beam, whereas there was a decrease in yield for the pure argon beam.

4.2.3 Heavy Species Enrichment on the Centerline of a Binary Beam

An increase in the concentration of the heavier species on the centerline of a binary beam has been observed by several investigators. The present results show that the argon concentration is about six times greater for the initial 1% Ar-99% H_2 case at 2000°K supply temperature. Klingelhöfer and Lohse (Ref. 13) show a 40-percent argon fraction for this initial mixture at room temperature source conditions. To help elucidate this discrepancy, a pair of runs shown in Fig. 18 were made at 285°K. These data suggest condensation or a more severe skimmer interaction effect than was observed at high temperature. The argon fraction in this case is 15 percent, which is shown in Fig. 19, along with the other measurements. The Ref. 13 data are about the same as the AEDC measurements at low source pressures. As the source pressure increases, however, the argon tends toward 40 percent of the flux.

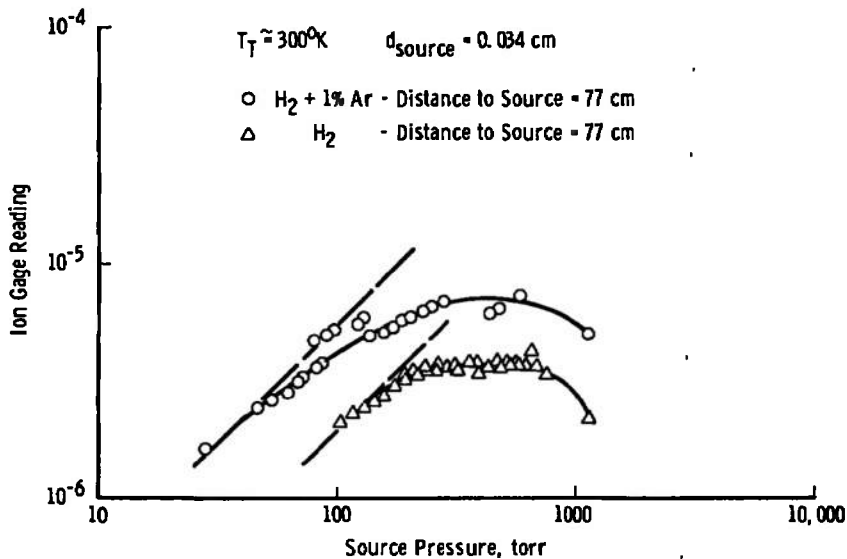


Figure 18. Room temperature beam intensity - ($H_2 + 1\% \text{ Ar}$) and H_2 beams.

The sampling technique in Ref. 13 was to use a 1-m-long, 3.3-cm-diam tube with an entrance aperture of 0.32 cm. Most of the beam enters and is pumped by a cold-trapped, 100-liter/sec mercury diffusion pump backed by a 12-liter/sec mercury diffusion pump and a mechanical pump. The foreline gas from the second diffusion pump was analyzed by conventional methods. It appears likely that this long sampling tube may tend to act like a closed volume such as the ion gage, particularly when the flux becomes large and the pressure increases. In such a situation, the partial density in terms of the flux into the volume will be

$$n = 4 \frac{\dot{n}}{\bar{u}} \sim \dot{n} \sqrt{M/T}$$

where \bar{u} is the mean thermal speed in static gas.

If the argon flux is assumed to be the 15 percent measured by the ion gage ($\dot{n}_{\text{Ar}} = 0.15 (\dot{n}_{H_2} + \dot{n}_{\text{Ar}})$), then the static concentration in the volume will be

$$\frac{n_{\text{Ar}}}{n_{\text{Ar}} + n_{H_2}} = \frac{\dot{n}_{\text{Ar}} \sqrt{40}}{\dot{n}_{\text{Ar}} \sqrt{40} + \dot{n}_{H_2} \sqrt{2}} = 0.44$$

This result is very close to the concentration reported, and it is shown in Fig. 19 as the "closed volume" line.

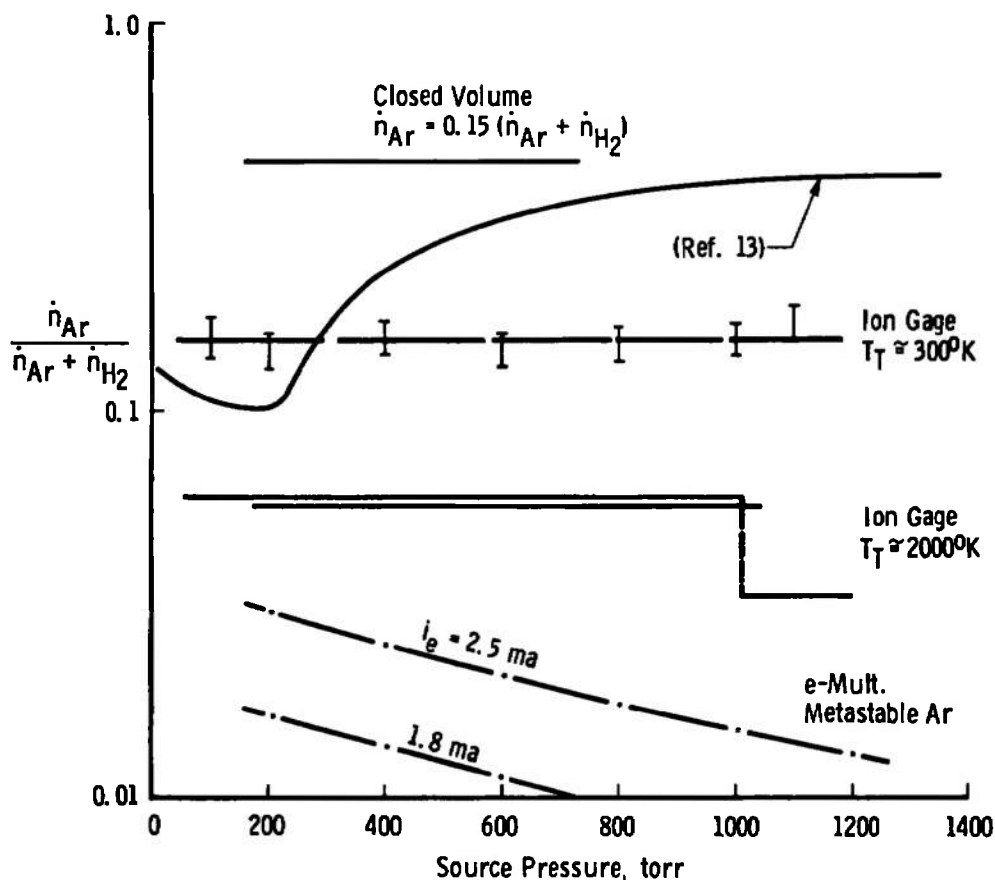


Figure 19. Argon enrichment in $H_2 + 1\%$ Ar beam.

To substantiate further a lower value for the enrichment effect, O'Keefe (Ref. 14) quotes a 9.4-percent argon fraction from a room temperature source for a 1% Ar-99% He mixture. This result is obviously consistent with the present measurements.

4.3 BEAM FLUX VARIATION IN THE AXIAL AND LATERAL DIRECTIONS

The ion gage was traversed across the beam at two axial positions in order to define the test region. Figure 14 shows the two profiles and an inverse-square variation from the centerline intensity at 69 cm. Unfortunately, the pressure chosen (1145 torr) was in the transition region attributed to skimmer interaction, where a significant variation of beam intensity occurs. However, it is reasonable to conclude that the test stream is fairly uniform over at least 1-cm diameter, and that the flux varies inversely with distance squared from the source. The diameter of near uniformity is about half the diameter based on the source-skimmer geometry.

5.0 CONCLUSIONS

The molecular beam method has been adapted into a facility useful for development or preflight testing of satellite-carried instruments. A mixed molecular beam of hydrogen and argon was formed from a high temperature source of hydrogen seeded with a small fraction of argon (1 percent). The argon was carried by the hydrogen to a speed over 6 km/sec, or an energy of nearly 8 ev. The concentration of argon in the beam was six times the source fraction, and the argon flux was over 2×10^{15} atoms/sec/cm². The beam width was at least 1 cm in diameter throughout the test chamber length of 30 cm.

As a satellite environment simulator, the facility produces a flux rate corresponding to a lower altitude of 290 km and an upper limit of 550 to 700 km based on the test chamber static gas pressure of 10^{-7} to 10^{-8} torr. The energy levels up to 8 ev may be compared to 4 for atomic nitrogen, 5 for atomic oxygen, 8 for nitrogen, and 10 for oxygen.

The beam size and the flow time of the order of 1 sec make full-scale tests of satellite-borne instruments practicable.

Future work should include obtaining somewhat higher stagnation temperatures and determining the performance of this system with other seed gases such as xenon, nitrogen, and oxygen. The measurement of aerodynamic forces is apparently feasible in a beam of this size by use of such a balance as described in Ref. 15.

REFERENCES

1. Becker, E. W. and Henkes, W. "Binary Mixtures for High Velocities." Zeitschrift für Physik, Vol. 146, 1956, pp. 320-332.
2. Abuaf, N. "Molecular Beams from Free Jets of Pure and Mixed Gases." Doctoral Dissertation, Princeton University, 1966. (University Microfilms 67-9589.)
3. Abuaf, N., Anderson, J. B., Andres, R. P., Fenn, J. B., and Miller, D. R. "Studies of Low Density Supersonic Jets." Fifth International Symposium on Rarefied Gas Dynamics, The University of Oxford, England, 1966, Vol. II, pp. 1317-1336.

4. Brown, R. F. and Heald, J. H., Jr. "Background Gas Scattering and Skimmer Interaction Studies Using a Cryogenically Pumped Molecular Beam Generator." Fifth International Symposium on Rarefied Gas Dynamics, The University of Oxford, England, 1966, Vol. II, pp. 1407-1424.
5. Locke, J. W. and French, J. B. "Critical Evaluation of the Metastable Time-of-Flight Technique for Obtaining Molecular Velocity Distributions." University of Toronto UTIAS Report No. 143, Toronto, Canada, December 1969.
6. Tempelmeyer, K. "Sorption Pumping of Hydrogen by Cryodeposits-Prediction of Sorption Capacity." AEDC-TR-69-270 (AD700981), February 1970.
7. Tempelmeyer, K. E., Dawbarn, R., and Young, R. L. "Sorption Pumping of Hydrogen by Carbon Dioxide Cryodeposits." Journal of Vacuum Science and Technology, Vol. 8, No. 4, July/August 1971, pp. 575-581.
8. Hagena, O. F. "Molecular Beam Production with an Impulse Operated Nozzle." Z. Agnew. Physics, Vol. 16, No. 3, 1963, pp. 183-187.
9. Dushman, Saul. "Scientific Foundations of Vacuum Technique." (Second Edition) John Wiley Publishing Co., New York, N.Y., 1962.
10. French, J. Barry. "Continuum-Source Molecular Beams." AIAA Journal, June 1965, Vol. 3, No. 6, pp. 993-1000.
11. Dawbarn, R., Arnold, F., and Stephenson, W. B. "Development of an Integrated Cryogenic Pumping System for Rocket Plume Studies." AEDC-TR-71-19 (AD880649), February 1971.
12. Arnold, F., Busby, M. R. and Dawbarn, Ronald. "Experimental Investigation of the Scattering of a Nitrogen Aerodynamic Molecular Beam from a Solid Nitrogen Surface." AEDC-TR-70-172 (AD712374), October 1970.
13. Klingelhöfer, R. and Lohse, P. "Production of Fast Molecular Beams Using Gaseous Mixtures." Conference on Molecular and Atomic Beams and Related Problems, Charlottesville, Virginia, 1963. Also in Physics of Fluids, Vol. 7, No. 3, March 1964, pp. 379-381.
14. O'Keefe, D. R. "Initial Performance Study of the UTIAS High Energy Molecular Beam Facility." UTIAS Tech Note No. 75, University of Toronto, Toronto, Canada.

15. Stephenson, W. B. and Whitfield, D. L. "Drag Measurement in a Low-Density Gas Stream." IEEE Transactions on Aerospace and Electronic Systems, Vol. AES-7, No. 6, November 1971, pp. 1131-1137. See also AEDC-TR-70-32 (AD704122).
16. U.S. Standard Atmosphere, 1962, December 1962, Washington, D. C.

APPENDIX A HYDROGEN SORPTION ON CO₂ FROST

References 6 and 7 show that hydrogen sorption by CO₂ frost can be expressed in isotherm form by the Dubinin-Radushkevich equation:

$$\log C = \log C^{\circ} - A T^2 [\log P/P_0]^2$$

The concentration C is the molar ratio of hydrogen to carbon dioxide in the frost. The maximum value, C° , corresponds to the ambient pressure, P , equal to the hydrogen vapor pressure, P_0 . The method of frost formation influences the value of C° ; in general, C° increases with the rate of formation (and probably the porosity or randomness) of the frost. This equation can be used to construct a family of curves, such as those in Fig. A-1, that are more or less parallel to the vapor pressure line for solid hydrogen. Very small changes in frost temperature result in large variation in equilibrium pressure.

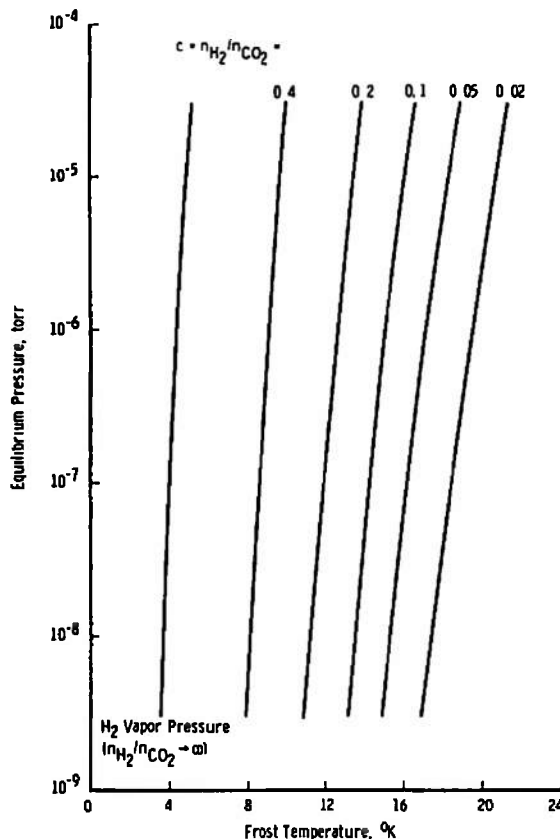


Figure A-1. H₂ pressure in equilibrium with CO₂ frost.

Another, and possibly more useful, form of plotting the equation is shown in Fig. A-2. Given a cryosurface temperature, one may determine the ratio of number of moles of CO_2 to H_2 that will provide the required equilibrium pressure. The Dubinin-Radushkevich equation results in a limit sorption ratio at the vapor pressure of hydrogen. However, it would appear that an asymptotic approach to the temperature corresponding to the pressure equal to vapor pressure would be more reasonable. Since the experimental data had a lower limit of about 12°K , it is not possible to decide the point.

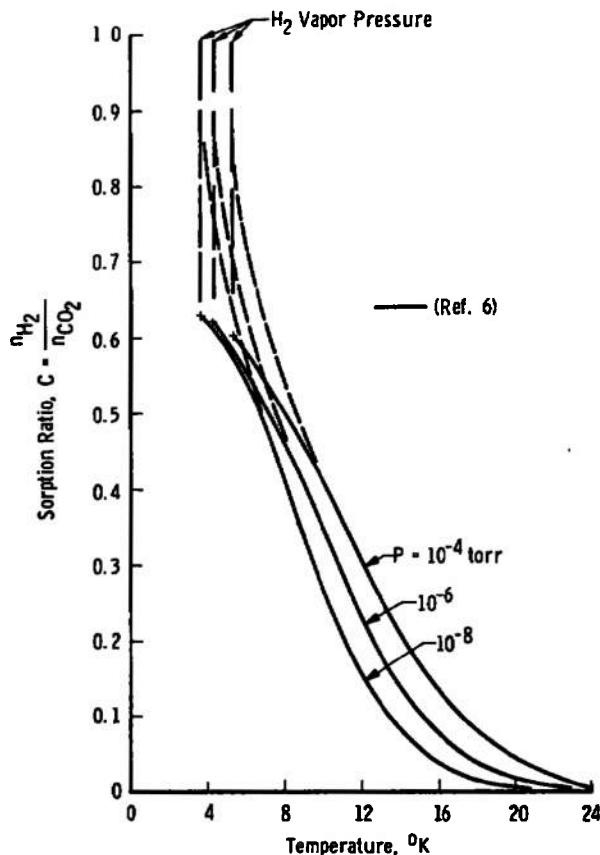


Figure A-2. Sorption of hydrogen in CO_2 frost.

NOMENCLATURE

A^*	Area of sonic orifice
a	Acoustic speed
E	Kinetic energy per molecule
e	Signal voltage of electron multiplier
k	Boltzmann constant
l	Distance from source
M	Molecular weight
m	Molecule mass
N_A	Avogadro number
\dot{N}	Number flux, sec^{-1}
n	Number density, cm^{-3}
\dot{n}	Number flux, $\text{cm}^{-2} \text{sec}^{-1}$
P	Pressure
$P_g, \Delta P_g$	Ionization gage ion currents, arbitrary units
S	Ion gage sensitivity
T_T	Stagnation temperature
U_{lim}	Limiting thermal velocity in an isentropic expansion
\bar{u}	Mean thermal speed in static gas
γ	Ratio of specific heats
ρ	Mass density
ω	Solid angle, steradians

SUBSCRIPTS

B	Beam
g	Ion gage
s	Source
T	Stagnation conditions

SUPERScript

$*$	Sonic point conditions
-----	------------------------